Tubulin polyglutamylation is essential for airway ciliary function through the regulation of beating asymmetry

Koji Ikegami[a,b,1], Showbu Sato[b], Kenji Nakamura[b], Lawrence E. Ostrowski[c], and Mitsutoshi Setou[a,b,1]

[a]Department of Molecular Anatomy, Molecular Imaging Advanced Research Center, Hamamatsu University School of Medicine, Hamamatsu, Shizuoka 431-3192, Japan; [b]Mitsubishi Kagaku Institute of Life Sciences, Machida, Tokyo 194-8511, Japan; and [c]Cystic Fibrosis/Pulmonary Research and Treatment Center, University of North Carolina, Chapel Hill, NC 27599

Edited* by J. Richard McIntosh, University of Colorado, Boulder, CO, and approved April 27, 2010 (received for review February 23, 2010)

Airway epithelial cilia protect the mammalian respiratory system from harmful inhaled materials by providing the force necessary for effective mucociliary clearance. Ciliary beating is asymmetric, composed of clearly distinguished effective and recovery strokes. Neither the importance of nor the essential components responsible for the beating asymmetry has been directly elucidated. We report here that the beating asymmetry is crucial for ciliary function and requires tubulin glutamylation, a unique posttranslational modification that is highly abundant in cilia. WT murine tracheal cilia have an axoneme-intrinsic structural curvature that points in the direction of effective strokes. The axonemal curvature was lost in tracheal cilia from mice with knockout of a tubulin glutamylation-performing enzyme, tubulin tyrosine ligase-like protein 1. Along with the loss of axonemal curvature, the axonemes and tracheal epithelial cilia from these knockout (KO) mice lost beating asymmetry. The loss of beating asymmetry resulted in a reduction of cilia-generated fluid flow in trachea from the KO mice. The KO mice displayed a significant accumulation of mucus in the nasal cavity, and also emitted frequent coughing- or sneezing-like noises. Thus, the beating asymmetry is important for airway ciliary function. Our findings provide evidence that tubulin glutamylation is essential for ciliary function through the regulation of beating asymmetry, and provides insight into the molecular basis underlying the beating asymmetry.

ciliary dyskinesia | ciliopathy | glutamylase | flagella | microtubule

Cilia are evolutionally conserved organelles that protrude from the cell surface and perform many different functions. Protists (e.g., paramecium) use these organelles for locomotion. Mammals use motile cilia to generate fluid flow on the cell surface. Mammalian airway epithelial cilia are part of the innate defense system that protects the respiratory system from inhaled harmful materials, including bacteria, viruses, and pollutants, by propelling mucus. The mucus flow is generated by the vigorous asymmetric beating of the cilia, which can be divided into effective strokes and recovery strokes (1). The importance of ciliary activity and mucociliary clearance in airway health has been well documented; for example, primary ciliary dyskinesia (PCD) is an inherited disease that can be caused by mutations resulting in a partial or complete loss of ciliary activity (2–4). In many cases of PCD, components of the dynein arms (the molecular motors responsible for cilia beating) are missing or defective (2–4). In contrast, fewer studies have investigated the mechanisms regulating the asymmetry of ciliary beating, and neither the importance of nor the essential components controlling the beating asymmetry has been elucidated.

The ciliary axoneme has a highly organized structure consisting of nine outer doublets and a central pair of tubulin fibers (i.e., a 9 + 2 structure) (5, 6). The major protein component of the ciliary axoneme, tubulin, undergoes glutamylation, a unique posttranslational modification (7, 8). Our group and others have recently identified glutamylation-performing enzymes known as glutamylases in tubulin tyrosine ligase (TTL)-like family members (9–12). The exact role of tubulin glutamylation in ciliary or flagellar function is unclear (13); however, the regulation of tubulin glutamylation is known to be critical for normal ciliary function (14, 15). The involvement of tubulin glutamylation in the regulation of ciliary or flagellar motilities has been suggested by studies in which a modification-specific antibody was injected into living cells (16–18); however, a recent study using a glutamylase-deficient protist revealed that glutamylases are not essential for ciliary motility in this system (19). To clearly investigate the role of tubulin glutamylation in the structure and motility of mammalian airway motile cilia, we generated knockout (KO) mice deficient in a tubulin glutamylase and analyzed both the in vivo phenotype and the effects on ciliary activity in vitro.

Results

Generation of *Ttll1*-KO Mice. Tubulin glutamylases belong to a family of proteins that contain a TTL domain. These TTL-like proteins are divided into classes based on their ability to initiate or elongate the glutamate chain and their preference for tubulin subunits (12). In this study, we disrupted the TTLL1 gene (TTL-like family member 1 gene) that codes for the catalytic subunit of a tubulin glutamylase (9, 11). TTLL1 has an initiating activity with a preference for α-tubulin, but also shows partial activity on β-tubulin (19). We replaced the exon containing the start codon of the TTLL1 gene with a TKneo cassette via homologous recombination (Fig. 1 *A* and *B*). Complete disruption of the TTLL1 gene was verified by detection of the loss of TTLL1 protein in lysates of respiratory organs, including the trachea and lung, from *Ttll1*-deficient homozygotes (Fig. 1*C*). Heterozygous matings produced littermates according to Mendelian law (Fig. 1*D*), indicating that the *Ttll1*-KO mice show neither embryonic nor postnatal lethality.

To examine the effect of the TTLL1 deletion on airway cilia, we first examined whether the TTLL1 deletion resulted in a loss of tubulin glutamylation using a monoclonal antibody, GT335, that recognizes both monoglutamylated and polyglutamylated tubulin (20). Immunolabeling of tracheal tissue sections revealed less staining with GT335 in the tracheal cilia of *Ttll1*-KO mice (Fig. 1*E*). Importantly, Western blot analyses revealed that the tracheal tissue lysates lost the majority of both glutamylated α- and β-tubulins (Fig. 1*F*). Other types of modifications, such as acetylation, detyrosination/tyrosination, and removal of penultimate glutamate (shown as Δ2), were not significantly affected by the deletion of TTLL1 (Fig. 1*F* and Fig. S1*A*). To directly examine whether the loss of glutamylated tubulin occurs in ciliary axonemes, we isolated axonemes from tracheas of WT and *Ttll1*-KO mice. Isolated ciliary axonemes

Author contributions: K.I. and M.S. designed research; K.I. and L.E.O. performed research; S.S. and K.N. contributed new reagents/analytic tools; K.I. and L.E.O. analyzed data; and K.I. and L.E.O. wrote the paper.

The authors declare no conflict of interest.

*This Direct Submission article had a prearranged editor.

[1]To whom correspondence may be addressed. E-mail: kikegami@hama-med.ac.jp or setou@hama-med.ac.jp.

This article contains supporting information online at www.pnas.org/lookup/suppl/doi:10.1073/pnas.1002128107/-/DCSupplemental.

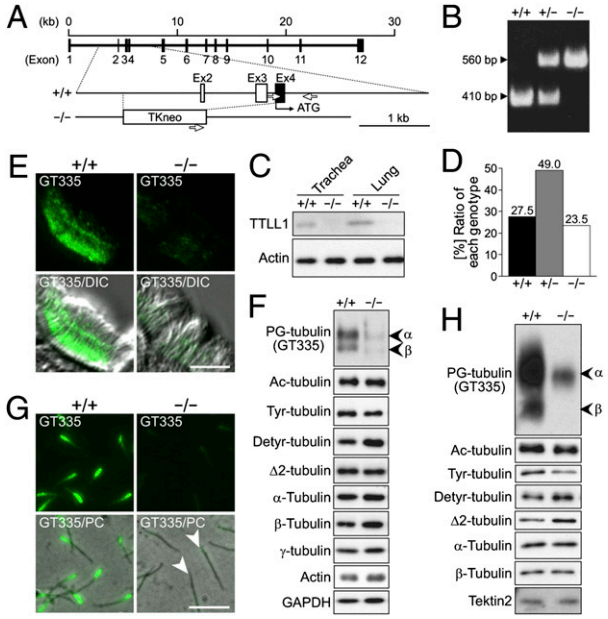

Fig. 1. Generation of *Ttll1*-KO mice. (*A* and *B*) Generation of *Ttll1*-deficient mice. (*A*) Exons 2–4 were replaced by a TKneo cassette through homologous recombination. (*B*) Each mouse was genotyped by PCR with primers depicted in *A* as white arrows. (*C*) Western blot analysis of TTLL1. TTLL1 protein was absent in the trachea and lung of *Ttll1*-deficent homozygote ($^{-/-}$) mice. (*D*) Results of heterozygous mating. The graph shows the ratio of each genotype [WT ($^{+/+}$), heterozygote ($^{+/-}$), or KO homozygote ($^{-/-}$)] born from heterozygous mating. In total, 690 animals obtained from 95 matings were genotyped. $P = 0.279$, χ^2 test. (*E*) Immunostaining of tracheal tissue section. WT cilia were stained by a mAb against glutamylated tubulin (GT335, green), whereas cilia from *Ttll1*-KO mice were not. (Scale bar: 5 μm.) (*F*) Detection of glutamylated tubulins in trachea. *Ttll1*-KO mice showed greatly reduced levels of glutamylated (PG) tubulin detected by the mAb GT335. Differences of other modifications—acetylation (Ac), tyrosination (Tyr), detyrosination (Detyr), and Δ2—were subtle when present. (*G*) Immunostaining of isolated ciliary axonemes with the mAb GT335. (Scale bar: 5 μm.) Arrowheads point to straight axonemes. (*H*) Detection of glutamylated tubulins and other modifications in isolated ciliary axonemes.

showed almost identical results to those for the whole-tissue lysates; ciliary axonemes isolated from *Ttll1*-KO mouse trachea were less stained with GT335 (Fig. 1*G*) and lost the majority of glutamylated α- and β-tubulins (Fig. 1*H*), with no significant alterations in the levels of other modifications (Fig. 1*H* and Fig. S1*B*).

Mice with a mutation in the PGs1 gene, which encodes a regulatory subunit of tubulin glutamylase (9, 11), show an abnormal development of sperm flagella (21). The *Ttll1*-KO mice displayed an almost identical phenotype to *PGs1*-KO mice; the sperm from *Ttll1*-KO mice had obviously shorter flagella than those from WT mice (Fig. S2). Despite the importance of tubulin glutamylation in flagellar construction, airway epithelial cilia were normally formed in the *Ttll1*-KO trachea (Fig. 1*E* and Fig. S3*A*). Consistent with the normal formation of tracheal epithelial cilia, there were no obvious ultrastructural abnormalities in tracheal ciliary axonemes of the *Ttll1*-KO mice; the basic 9 + 2 axonemal structure was normal (Fig. S3*B*), the numbers of inner and outer dynein arms were not decreased (Fig. S3 *C* and *D*), and structures surrounding the central doublet microtubules were not missing (Fig. S3*E*).

Loss of Axonemal Curvature in *Ttll1*-KO Mouse Tracheal Epithelial Cilia. Although the foregoing investigations demonstrated no obvious structural changes in cilia from the *Ttll1*-KO mice, we did observe an apparent alteration in the shape of the *Ttll1*-KO ciliary axonemes. Of special interest, we noticed that ciliary axonemes isolated from *Ttll1*-KO mice were often straightened (Fig. 1*G*; arrowheads), whereas those from WT mice were typically curved (Fig. 1*G*). To eliminate possible artifacts introduced by the immunostaining processes, we directly observed the shape of axonemes after isolation and quantified the bend angle by assuming the axoneme to be a simple arc (Fig. S4). WT axonemes showed a clear curvature (Fig. 2*A*) with an average bend angle of about 50 degrees (Fig. 2 *B* and *C*). In contrast, a major portion of *Ttll1*-KO axonemes lost the curvature (Fig. 2*A*, arrows). The bend angles of *Ttll1*-KO axonemes were concentrated at <40 degrees (Fig. 2 *B* and *C*).

A possible explanation for this difference is that the axonemal curvature observed in the WT axonemes results from fixation of the axoneme in an active position of the ciliary beating cycle, which can result from strong rigor states of dynein motors (22, 23). To address this issue, we produced axonemes in a relaxed state by exposing them to low concentrations of ATP (<10 μM), as reported previously (22, 23). In our protocol, 2 μM ATP caused the smallest average bend angle (Fig. S5). Even under this condition, WT axonemes retained a similar degree of curvature, whereas *Ttll1*-KO axonemes remained in a more straightened form (Fig. 2 *D* and *E*). This suggests that the axonemal curvature is a structurally intrinsic property of the axoneme and is independent of dynein rigor state. The loss of curvature was not accompanied by altered axonemal length in the *Ttll1*-KO tracheal cilia (Fig. 2*F*). Based on these two parameters, representative axonemes from WT and *Ttll1*-KO mice clearly showed a loss of structural curvature in the *Ttll1*-KO axoneme (Fig. 2*G*). Taken together, our findings demonstrate that tubulin glutamylation is required for the structural curvature of ciliary axonemes, which is independent of dynein-rigor bridges and inherent in axoneme.

Loss of Beating Asymmetry in ATP-Reactivated Ciliary Axonemes of *Ttll1*-KO Mice. We next examined the relationship between the direction of the axoneme-intrinsic structural curvature and the

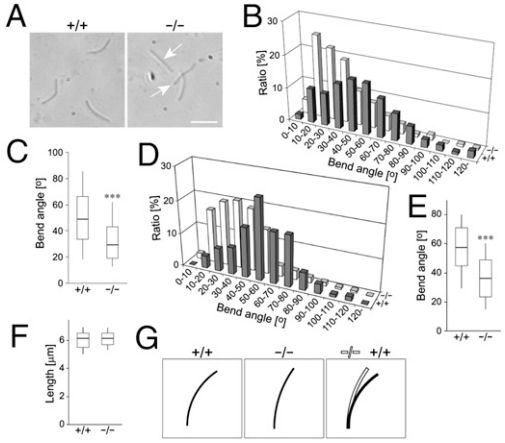

Fig. 2. Loss of structural curvature in ciliary axonemes of *Ttll1*-KO mice. (*A*) Phase-contrast micrograph of isolated ciliary axonemes. Arrows point to straightened axonemes in the *Ttll1*-KO preparation. (Scale bar: 5 μm.) (*B* and *C*) Bend angles of isolated ciliary axonemes. Both the histogram (*B*) and the boxplot (*C*) of bend angles show that the majority of *Ttll1*-KO axonemes had bend angles <40 degrees. In *C*, data are presented as median ± quartile (box) and 90th percentile (bars). ***$P < 0.001$, Mann-Whitney *U* test [$n = 621$ ($^{+/+}$), 557 ($^{-/-}$)]. (*D* and *E*) Bend angles of relaxed axonemes. Both the histogram (*D*) and the boxplot (*E*) of bend angles show that the majority of *Ttll1*-KO axonemes had bend angles <40 degrees. In *E*, data are presented as median ± quartile (box) and 90th percentile (bars). ***$P < 0.001$, Mann-Whitney *U* test [$n = 244$ ($^{+/+}$), 186 ($^{-/-}$)]. (*F*) Boxplot of lengths of ciliary axonemes. Data are presented as median ± quartile (box) and 90th percentile (bars). No statistically significant difference was detected. (*G*) Representative shape of axonemes depicted from medians of angle and length. The overlay image clearly shows the reduced bend angle of the *Ttll1*-KO axonemes.

asymmetric ciliary waveform. To accomplish this, we manipulated ciliary motility in isolated ciliated cortices prepared from murine trachea. Axonemes were first converted to a relaxed state by exposing the ciliated cortex to a low concentration of ATP. Under this condition, all cilia curved in one direction (Fig. 3*A* and Movie S1). We then reactivated the cilia by replacing the solution with a 0.1 mM ATP-containing solution. The reactivated cilia generated effective strokes in the same direction as the curvature direction (Fig. 3*A*, Movie S1). Thus, the direction of the axoneme-intrinsic structural curvature points to the direction of asymmetric beating (Fig. 3*B*).

Based on these data, we hypothesized that tubulin glutamylation is essential for the establishment of asymmetry in ciliary beating, given that WT axonemes had an intrinsic structural curvature that pointed in the direction of the effective stroke (Fig. 3*B*) and that the curvature was lost in axonemes of *Ttll1*-KO tracheal cilia (Fig. 2 *D*, *E*, and *G*). To test this hypothesis, we prepared isolated ciliary axonemes from WT and *Ttll1*-KO tracheas, reactivated the axonemes by adding ATP, and compared their motilities. The use of isolated axonemes for analysis avoided some of the difficulties of investigating ciliary beating asymmetry in tracheal preparations. For example, the fluid flow generated by the large number of cilia on tracheal epithelia could positively affect (i.e., enhance or amplify) the ciliary beating asymmetry (24), or rows of neighboring cilia could interfere with the beating pattern of adjacent cilia (25, 26).

Thus, we first examined whether ATP-reactivated *Ttll1*-KO axoneme lost beating asymmetry. We recorded the motility of 1 mM ATP-reactivated axonemes by means of a microscope equipped with a high-speed digital camera (Movie S2 and Movie S3). Frame-by-frame photographs are shown in Fig. 3*C*; kymographs of the movies are shown in Fig. 3*D*. To quantify the axoneme motility, we wrote a simple software program that allowed us to map the position of the ciliary tips in each frame. Trajectories, in which the beating plane was fitted on the *y*-axis, are shown in Fig. 3*E* (*Top*). We expanded the *y*-axial trajectory on a time axis (Fig. 3*E*, *Middle*). From the trajectory, we calculated *y*-axial velocity (Fig. 3*E*, *Bottom*). The ratio of maximum velocities between effective and recovery strokes was significantly decreased and almost reached 1 in *Ttll1*-KO axonemes (Fig. 3*F*), demonstrating that the *Ttll1*-KO axonemes lost beating asymmetry (i.e., the effective and recovery strokes were similar). Ciliary axonemes isolated from *Ttll1*-KO mice also showed a 1.5-fold increase in ciliary beating frequency compared with ciliary axonemes from WT mice (Fig. 3*G*). Our findings indicate that tubulin glutamylation is required for generating the asymmetry between the effective and recovery strokes in the beating pattern of ciliary axonemes.

Loss of Ciliary Beating Asymmetry in *Ttll1*-KO Trachea. We next examined whether the beating asymmetry of intact cilia is affected in tracheas from *Ttll1*-KO mice. For this experiment, isolated tracheas were placed in organ culture and the tips of the cilia were labeled with a diluted solution of Indian ink. Ciliary motility was recorded and analyzed as above (Movie S4 and Movie S5). Frame-by-frame photographs of the movies are shown in Fig. 4*A*. The direction of the effective (E) and recovery (R) strokes were determined by the orientation of the trachea. Kymographs of the movies are shown in Fig 4*B*. Analyses of ciliary beating pattern were performed with the same procedure used to analyze axonemal beating pattern (Fig. 4*C*). The ratio between the velocities of the effective stroke and recovery stroke also was significantly decreased in *Ttll1*-KO cilia (Fig. 4*D*). The ciliary beating frequency was also 1.5-fold higher in *Ttll1*-KO mice than in WT mice (Fig. 4*E*). Thus, the results obtained using intact tracheas are identical to the results obtained with isolated axonemes, also supporting the conclusion that tubulin glutamylation is essential for the establishment of ciliary beating asymmetry.

Primacy Ciliary Dyskinesia–Like Respiratory Phenotypes in *Ttll1*-KO Mice. It is widely known that defects in ciliary motility, usually described as partial or complete lack of activity, impair the ability of cilia to generate proper fluid flow and result in the phenotypic features of PCD (27–30). In contrast, there are no reports exam-

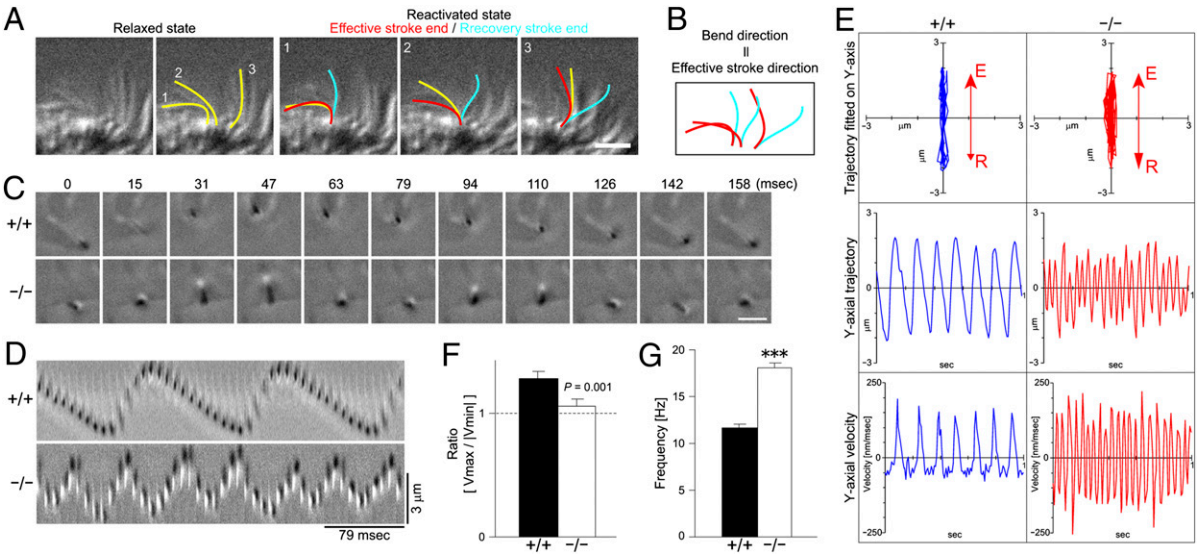

Fig. 3. Loss of beating asymmetry in *Ttll1*-KO ciliary axonemes. (*A* and *B*) Relationship between bend direction and beating direction. (*A*) Three representative cilia are highlighted. In the relaxed state, all cilia retained bends to the left (yellow). After reactivation, the cilia beat to the left (blue to red). (Scale bar: 5 μm.) (*B*) Note that the bend direction is the same as the direction of the effective stroke. (*C*) Time-lapse photography of ATP-reactivated ciliary axoneme. (Scale bar: 3 μm.) (*D*) Kymograph of an ATP-reactivated ciliary axoneme. (*E*) Analyses of axonemal motility. The beating plane of the original trajectory was fitted on the *y* axis (*Top*). The *y*-axial trajectory was plotted as a time function (*Middle*). The velocity in the *y*-direction was plotted against time (*Bottom*). (*F*) Distinction between effective and recovery strokes. The ratio between the maximum and minimum velocity was decreased significantly in axonemes from the *Ttll1*-KO mice and approached a value of 1, indicating a symmetric beating pattern [$P = 0.001$, one-way ANOVA; $n = 56$ ($^{+/+}$), 65 ($^{-/-}$)]. (*G*) Frequency of axonemal beating. Axonemes isolated from *Ttll1*-KO mice showed a significantly increased ciliary beating frequency compared with axonemes isolated from WT animals ($P < 0.001$, one-way ANOVA).

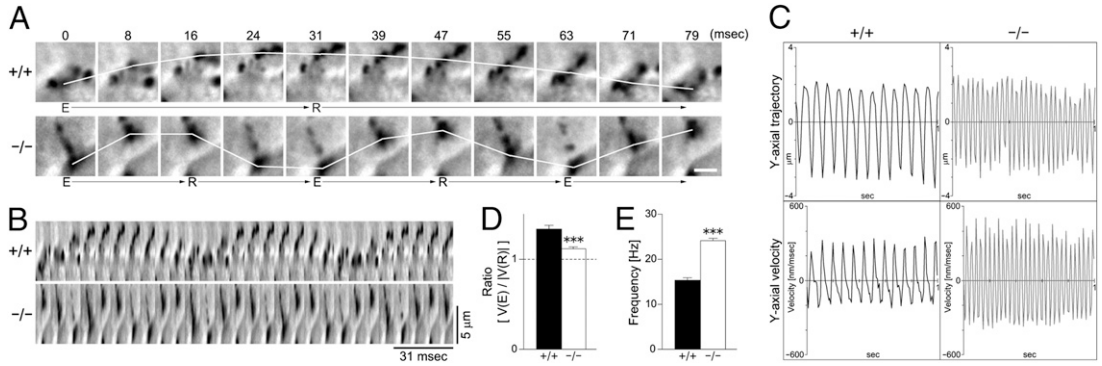

Fig. 4. Loss of beating asymmetry of tracheal epithelial cilia in *Ttll1*-KO mice. (*A*) Time-lapse photography of labeled cilia. The white line shows a trace of ciliary motility during the effective (E) and recovery (R) strokes. (Scale bar: 3 μm.) (*B*) Kymograph of ciliary strokes. (*C*) Analyses of ciliary motility. The ciliary trajectory was plotted as a time function after being fitted onto the *y* axis (*Upper*). The velocity in the *y*-direction was plotted against time (*Lower*). (*D*) Distinction between effective and recovery strokes. The ratio of velocities between effective and recovery strokes was significantly decreased in *Ttll1*-KO cilia ($P < 0.001$, one-way ANOVA; $n = 40$). (*E*) Frequency of ciliary beating. *Ttll1*-KO cilia showed a significantly higher beating frequency than WT cilia ($P < 0.001$, one-way ANOVA).

ining the effect of defects in ciliary beating asymmetry on ciliary function. We thus examined whether the observed loss of ciliary beating asymmetry results in defective ciliary function in *Ttll1*-KO mice. We recorded and analyzed the cilia-generated fluid flow over the tracheal surface using small polystyrene beads (Fig. 5*A* and Movie S6 and Movie S7). Consistent with the loss of ciliary beating asymmetry, the rate of cilia-driven transport was significantly reduced in *Ttll1*-KO mice tracheas (Fig. 5*B*). The reduced flow velocity in the *Ttll1*-KO tracheas was accompanied by slightly impaired intercellular coordination of beating orientation (Fig. 5*C*). Intracellular coordination of beating orientation, determined by the orientation of basal feet, was not affected (Fig. 5 *D* and *E*).

In humans with PCD and mouse models alike, defects in mucociliary clearance result in a high incidence of rhinosinusitis. Thus, we examined whether the *Ttll1*-KO mice exhibited any evidence of mucus accumulation in the nasal cavity. Paraffin sections of the nasal cavity from WT and *Ttll1*-KO mice were stained with Alcian blue to clearly detect any accumulated mucus. Alcian blue–positive mucus was clearly detected in the nasal cavity and sinuses of *Ttll1*-KO mice,

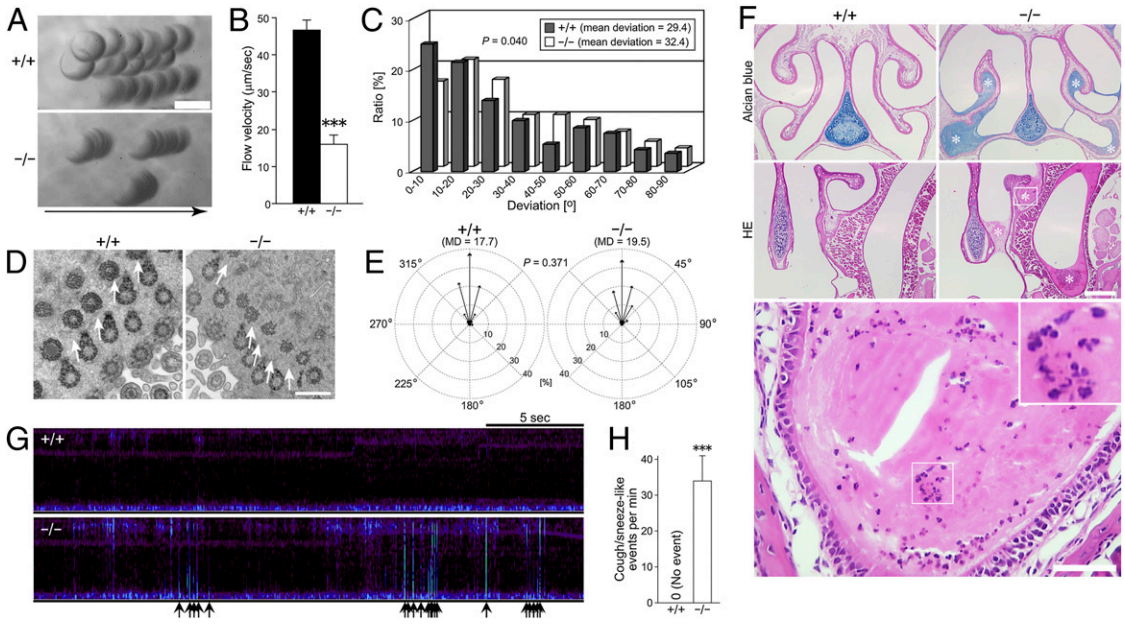

Fig. 5. Ciliary dysfunction, rhinosinusitis, and respiratory defects in *Ttll1*-KO mice. (*A* and *B*) Cilia-generated flow. In *A*, 500-ms trajectories of polystyrene beads deposited on the tracheal surface are depicted in 66-ms intervals. (Scale bar: 10 μm.) Quantified data are shown in *B*. The velocity of each bead was estimated by dividing the width of the field of view (50 μm) by the time each individual bead takes to pass through the field. Data are presented as mean ± SEM [$n = 15$ ($^{+/+}$), 10 ($^{-/-}$)]. ***$P < 0.001$, one-way ANOVA. (*C*) Orientation of ciliary beating. The mean deviation showed a slight, but statistically significant increase in *Ttll1*-KO mice. *P* values were analyzed with the Mann-Whitney *U* test [$n = 279$ ($^{+/+}$), 304 ($^{-/-}$)]. (*D* and *E*) Orientation of ciliary basal feet. (*D*) The basal feet of both WT and *Ttll1*-KO mice point in the same direction (white arrows) in the transmission electron microscopy (TEM) micrographs. (*E*) Rose diagrams of basal foot orientation. There was no statistically significant difference using the Mann-Whitney *U* test [$n = 121$ ($^{+/+}$), 146 ($^{-/-}$)]. MD, mean deviation. (*F*) Alcian blue (*Top*) and H&E (*Middle*) staining of nasal cavity. In *Ttll1*-KO mice, accumulated mucus was clearly visible (asterisks), whereas WT mice showed no mucus accumulation. (*Bottom*) A magnified photograph of the boxed region of the H&E-stained KO sample. (*Inset*) Neutrophils in the nasal cavity of a *Ttll1*-KO mouse. [Scale bars: 0.4 mm (*Top* and *Middle*), 50 μm (*Bottom*).] (*G* and *H*) Coughing-/sneezing-like phenotypes in *Ttll1*-KO mice. (*G*) Strong spikes (arrows) were observed only in spectrograms recorded from KO animals. (*H*) Quantification of the frequency of coughing-/sneezing-like noises observed in *Ttll1*-KO mice. ***$P < 0.001$, one-way ANOVA ($n = 3$). No coughing-/sneezing-like noises were recorded from WT mice.

whereas no evidence of mucus accumulation was observed in WT mice (Fig. 5*F*, *Upper*). Staining with H&E revealed many infiltrating neutrophils are present in the accumulating mucus (Fig. 5*F*, *Lower*, *Inset*), providing additional evidence of rhinosinusitis.

In addition to rhinosinusitis, patients with PCD typically present with chronic cough (31). Thus, we examined the respiratory phenotypes of *Ttll1*-KO mice. We observed that they frequently made coughing- or sneezing-like noises (Movie S8 and Movie S9), whereas WT animals were mostly silent (Movie S10). To evaluate the severity of the phenotype, we counted the frequency of coughing- or sneezing-like noises. We recorded 1-min audio files from WT and *Ttll1*-KO mice and displayed the data as a sound spectrogram. The coughing-/sneezing-like noises are clearly shown in the spectrogram as strong spikes (Fig. 5*G*, arrows). By counting the spikes, we found that *Ttll1*-KO mice made the coughing-/sneezing-like noises about 30 times per minute (Fig. 5*H*). The incidence of the phenotype was 100%, because we were able to correctly identify *Ttll1*-KO homozygotes by the presence of coughing- or sneezing-like noises before performing PCR-based genotyping. The onset of this coughing phenotype was at least 2 weeks after birth.

To confirm this observation, we examined another mouse model of PCD in which a deletion was introduced into the gene coding for axonemal dynein intermediate chain Dnaic1 (32). Two groups of animals were examined by similar techniques; eight of nine PCD animals produced frequent coughing-/sneezing-like sounds (Audio S1), whereas the control animals did not (Audio S2). An investigator blinded to the genotype identified 18/19 animals correctly after listening to a 1-min audio recording. Thus, similar to PCD patients, mice with defects in mucociliary clearance apparently use coughing/sneezing as a backup mechanism to clear their airways.

Discussion

Our findings demonstrate that generation of an asymmetric ciliary beating pattern requires axonemal tubulin glutamylation. An important question that remains is how tubulin glutamylation results in ciliary beating asymmetry. At least two hypotheses can be raised. First, tubulin glutamylation per se might be asymmetrically distributed. An asymmetric distribution of glutamylated tubulin has been reported in murine sperm flagellar axonemes. Glutamylated tubulin is distributed predominantly in axonemal outer doublets 1, 5, and 6 (33). In a ciliary axoneme, these three doublets are located closest to the plane of beating, with doublets 5 and 6 positioned on the side of the effective stroke direction and doublet 1 on the opposite side—that is, the side of the recovery stroke direction (1). Thus, the centroid of tubulin glutamylation is not in the center of the axoneme, but rather is shifted in the direction of the effective stroke and may produce asymmetry in the beating pattern (Fig. S6). In this model, the loss of glutamylation would eliminate the asymmetry and possibly prevent the asymmetric beating pattern. A second possibility is that the ciliary axoneme per se could have an underlying architectural asymmetry. For example, *Chlamydomonas* flagella have a special beak-like structure in outer doublets 1, 5, and 6 (34, 35); in addition, the inner dynein arm compositions are different on doublets 1 and 9 (35). If these or other structures required interaction with glutamylated tubulin for proper localization and functioning, then the loss of tubulin glutamylation could result in a loss of structural asymmetry. This type of asymmetry has not been reported for mammalian cilia, however.

We also have found that ciliary axonemes have an intrinsic structural curvature dependent on tubulin glutamylation (Fig. 2). A microphotograph of a preparation of ciliary axonemes isolated from porcine trachea showing a bending tendency of the axonemes was published in 1986 (36). The mechanism for this inherent ciliary curvature had not been studied until now, however, because it was interpreted as simply an "instantly-fixed" shape of the normal ciliary beating cycle (37), similar to that observed in rigor waves of sperm flagella (22, 23). Our data demonstrate that the curvature is independent of the rigor state of the dynein motors (Fig. S5). A number of previous reports support our findings. For example, ATP-relaxed sperm flagella retain a curved shape with an average bend angle of 50 degrees (23), which is equal to the median bend angle of relaxed ciliary axonemes in the present study. Immotile human airway epithelial cilia that lack the outer axonemal dynein heavy chain DNAH5 retain their structural curvature (38). Moreover, *Ktu*-KO mice that completely lack outer dynein arms and have a partial deficit of inner dynein arms have curved cilia, even though the cilia are completely immotile (39). Thus, the structural curvature of ciliary axoneme is neither a "still image" of the normal ciliary beating cycle nor a result of dynein rigor bridges. The inherent structural curvature is consistent with the concept that the resting position of beating cilia is at the end of the effective stroke, that is, the most bent position (40). The axoneme-intrinsic bending force generating the axonemal curvature could bias beating toward the direction of curvature, as suggested by the finding that external forces (i.e., flow) generate beating asymmetry (24).

In this study, we provide direct evidence of the importance of ciliary beating asymmetry in ciliary function. The *Ttll1*-KO mice exhibited many of the phenotypic traits of PCD, including a reduced rate of cilia-generated flow (Fig. 5 *A* and *B*), defective formation of sperm flagella, and development of rhinosinusitis (Fig. 5 *F–H*). Interestingly, however, they did not present other phenotypes commonly seen in mouse models of PCD. In particular, we found no animal with situs inversus or severe hydrocephalus among the more than 50 animals observed. This perhaps can be explained by the fact that *Ttll1*-KO cilia remained motile. Specialized nodal cilia, which determine the left-right axis of the body (41), might not require TTLL1 to be functional. Because ciliary beating asymmetry and cilia-generated flow were partially maintained in the trachea (Figs. 4*D* and 5*C*), sufficient fluid flow could remain in the brain ventricles to prevent the development of hydrocephalus. The residual flow also could explain the mildness of the beating orientation impairment. Alternatively, the presence of residual tubulin glutamylation might explain the mildness of the phenotypes observed, given that the *Ttll1*-KO did not result in complete loss of tubulin glutamylation (Fig. 1 *E–H*).

Two additional findings warrant mention. First, *Ttll1*-KO mice demonstrated grossly reduced levels of both α- and β-tubulin glutamylation in respiratory ciliary axonemes (Fig. 1 *F* and *H*), although TTLL1 was originally isolated from murine brain as a catalytic subunit of a glutamylase complex with a preference for modifying α-tubulin (9, 11). This is perhaps not surprising, however, because *Tetrahymena* TTLL1 has detectable levels of β-tubulin glutamylase activity (19) and accounts for both α- and β-tubulin glutamylation in the cytoskeletal fraction of *Tetrahymena* (19). TTLL1 might have different specificities in different species or cell types, or in different subcellular locations. Second, *Ttll1*-KO cilia had an increased beating frequency (Fig. 4*E*). A similar increase in beating frequency has been reported in cases of human PCD caused by mutations in the outer axonemal dynein heavy chain DNAH11 (42, 43). In contrast, ciliary or flagellar beating frequency is decreased in *Tetrahymena* with a reduced level of glutamylated β-tubulin (44) and also in *Chlamydomonas* that grossly loses glutamylated α-tubulin (45). However, the loss of glutamylated tubulin resulted in an increase in microtubule-sliding activity of inner arm dyneins in mutants lacking outer dynein arms. These results indicate that many complex interactions between glutamylated α- and β-tubulins and inner and outer dynein arms are likely involved in the regulation of ciliary beating frequency.

The ciliary (and flagellar) axoneme has a highly complex, organized structure (5, 6). Furthermore, the axoneme is composed of hundreds of proteins present in widely varying amounts (46, 47). Some previous studies have suggested that the structural asymmetry might be responsible for the asymmetry of the beating cycle (34, 35).

In addition, some mathematical simulations have been performed (24–26, 48). These hypotheses have not yet been tested by loss-of-function models, however. Our work demonstrates, by means of a loss-of-function animal model, that ciliary beating asymmetry depends on tubulin glutamylation. These findings provide insight into the molecular basis responsible for generating the effective and recovery strokes in the ciliary beating cycle.

Materials and Methods

Animals. The *Ttll1*-KO mice were newly developed (Fig. 1*A*). The conditional *Dnaic1*-KO mice were established previously (32). All animal use experiments followed protocols approved by the Animal Care and Use Committees of the respective institutions.

Preparation and Reactivation of Ciliated Cortices and Cilia. Ciliated cortices were prepared from murine trachea as described previously (49) with some modifications. Cilia isolation and reactivation were carried out as described previously (36) with an extensive scale-down of procedures. Immunoblotting and immunostaining were performed as described previously (50, 51). Bend angles were calculated as shown in Fig. S4.

Analyses of Ciliary Motility, Beating Orientation, and Cilia-Driven Flow. Motilities of reactivated axonemes or intact cilia were recorded with a high-speed CCD camera. Traces of ciliary activity were obtained by tracking the coordinates of the ciliary tips using a customized software program. The slope of the beating plane was used for the analysis of beating orientation. Analyses were performed as described previously (29). Ciliary transport on the surface of intact tracheas was analyzed in transient organ culture.

Other Methods and Detailed Procedures. The methods and techniques used are described in more detail in *SI Materials and Methods*.

ACKNOWLEDGMENTS. We thank C. Janke (Institut Curie) for the generous gift of monoclonal antibody GT335; R. Kamiya (University of Tokyo) for valuable discussions; M. Anbai for developing analysis software; and S. Kamijo, M. Matsuo, R. Suzuki-Migishima, T. Hino, and Y. Hinohara (Mitsubishi Kagaku Institute of Life Sciences); N. Suzuki and C. Nagashima (Hamamatsu University School of Medicine); and other Setou Laboratory members, especially S. Taira, K. Yasutake, K. Ohtsu, and M. Ogawa, for their technical assistance. This work was supported by grants-in-aid from the Japan Society for the Promotion of Science (to M.S.).

1. Gibbons IR (1961) The relationship between the fine structure and direction of beat in gill cilia of a lamellibranch mollusc. *J Biophys Biochem Cytol* 11:179–205.
2. Afzelius BA (1976) A human syndrome caused by immotile cilia. *Science* 193:317–319.
3. Ferkol T, Leigh M (2006) Primary ciliary dyskinesia and newborn respiratory distress. *Semin Perinatol* 30:335–340.
4. Morillas HN, Zariwala M, Knowles MR (2007) Genetic causes of bronchiectasis: Primary ciliary dyskinesia. *Respiration* 74:252–263.
5. Nicastro D, et al. (2006) The molecular architecture of axonemes revealed by cryoelectron tomography. *Science* 313:944–948.
6. Sui H, Downing KH (2006) Molecular architecture of axonemal microtubule doublets revealed by cryo-electron tomography. *Nature* 442:475–478.
7. Eddé B, et al. (1990) Posttranslational glutamylation of α-tubulin. *Science* 247:83–85.
8. Alexander JE, et al. (1991) Characterization of posttranslational modifications in neuron-specific class III beta-tubulin by mass spectrometry. *Proc Natl Acad Sci USA* 88:4685–4689.
9. Janke C, et al. (2005) Tubulin polyglutamylase enzymes are members of the TTL domain protein family. *Science* 308:1758–1762.
10. Ikegami K, et al. (2006) TTLL7 is a mammalian β-tubulin polyglutamylase required for growth of MAP2-positive neurites. *J Biol Chem* 281:30707–30716.
11. Ikegami K, et al. (2007) Loss of α-tubulin polyglutamylation in ROSA22 mice is associated with abnormal targeting of KIF1A and modulated synaptic function. *Proc Natl Acad Sci USA* 104:3213–3218.
12. van Dijk J, et al. (2007) A targeted multienzyme mechanism for selective microtubule polyglutamylation. *Mol Cell* 26:437–448.
13. Ikegami K, Setou M (2010) Unique post-translational modifications in specialized microtubule architecture. *Cell Struct Funct* 35:15–22.
14. Bulinski JC (2009) Tubulin posttranslational modifications: A pushmi-pullyu at work? *Dev Cell* 16:773–774.
15. Wloga D, et al. (2010) Hyperglutamylation of tubulin can either stabilize or destabilize microtubules in the same cell. *Eukaryot Cell* 9:184–193.
16. Million K, et al. (1999) Polyglutamylation and polyglycylation of α- and β-tubulins during *in vitro* ciliated cell differentiation of human respiratory epithelial cells. *J Cell Sci* 112:4357–4366.
17. Gagnon C, et al. (1996) The polyglutamylated lateral chain of α-tubulin plays a key role in flagellar motility. *J Cell Sci* 109:1545–1553.
18. Rosenbaum J (2000) Cytoskeleton: Functions for tubulin modifications at last. *Curr Biol* 10:R801–R803.
19. Wloga D, et al. (2008) Glutamylation on α-tubulin is not essential but affects the assembly and functions of a subset of microtubules in *Tetrahymena thermophila*. *Eukaryot Cell* 7:1362–1372.
20. Wolff A, et al. (1992) Distribution of glutamylated α and β-tubulin in mouse tissues using a specific monoclonal antibody, GT335. *Eur J Cell Biol* 59:425–432.
21. Campbell PK, et al. (2002) Mutation of a novel gene results in abnormal development of spermatid flagella, loss of intermale aggression and reduced body fat in mice. *Genetics* 162:307–320.
22. Gibbons BH, Gibbons IR (1974) Properties of flagellar "rigor waves" formed by abrupt removal of adenosine triphosphate from actively swimming sea urchin sperm. *J Cell Biol* 63:970–985.
23. Penningroth SM, Cheung A, Olehnik K, Koslosky R (1982) Mechanochemical coupling in the relaxation of rigor-wave sea urchin sperm flagella. *J Cell Biol* 92:733–741.
24. Guirao B, Joanny JF (2007) Spontaneous creation of macroscopic flow and metachronal waves in an array of cilia. *Biophys J* 92:1900–1917.
25. Gueron S, Levit-Gurevich K, Liron N, Blum JJ (1997) Cilia internal mechanism and metachronal coordination as the result of hydrodynamical coupling. *Proc Natl Acad Sci USA* 94:6001–6006.
26. Gueron S, Levit-Gurevich K (1998) Computation of the internal forces in cilia: Application to ciliary motion, the effects of viscosity, and cilia interactions. *Biophys J* 74:1658–1676.
27. Ibañez-Tallon I, Gorokhova S, Heintz N (2002) Loss of function of axonemal dynein Mdnah5 causes primary ciliary dyskinesia and hydrocephalus. *Hum Mol Genet* 11:715–721.
28. Tanaka H, et al. (2004) Mice deficient in the axonemal protein Tektin-t exhibit male infertility and immotile-cilium syndrome due to impaired inner arm dynein function. *Mol Cell Biol* 24:7958–7964.
29. Lechtreck KF, Delmotte P, Robinson ML, Sanderson MJ, Witman GB (2008) Mutations in *Hydin* impair ciliary motility in mice. *J Cell Biol* 180:633–643.
30. Fernandez-Gonzalez A, Kourembanas S, Wyatt TA, Mitsialis SA (2007) Mutation of murine adenylate kinase 7 underlies a primary ciliary dyskinesia phenotype. *Am J Respir Cell Mol Biol* 40:305–313.
31. Chilvers MA, O'Callaghan C (2000) Case 1: Assessment: Chronic wet cough. *Paediatr Respir Rev* 1:81–82.
32. Ostrowski LE, et al. (2009) Conditional deletion of *Dnaic1* in a murine model of primary ciliary dyskinesia causes chronic rhinosinusitis. *Am J Respir Cell Mol Biol* 10.1165/rcmb.2009-0118OC.
33. Fouquet JP, Prigent Y, Kann ML (1996) Comparative immunogold analysis of tubulin isoforms in the mouse sperm flagellum: Unique distribution of glutamylated tubulin. *Mol Reprod Dev* 43:358–365.
34. Hoops HJ, Witman GB (1983) Outer doublet heterogeneity reveals structural polarity related to beat direction in *Chlamydomonas* flagella. *J Cell Biol* 97:902–908.
35. Bui KH, Sakakibara H, Movassagh T, Oiwa K, Ishikawa T (2009) Asymmetry of inner dynein arms and inter-doublet links in *Chlamydomonas* flagella. *J Cell Biol* 186:437–446.
36. Hastie AT, et al. (1986) Isolation of cilia from porcine tracheal epithelium and extraction of dynein arms. *Cell Motil Cytoskeleton* 6:25–34.
37. Dentler WL, LeCluyse EL (1982) Microtubule capping structures at the tips of tracheal cilia: Evidence for their firm attachment during ciliary bend formation and the restriction of microtubule sliding. *Cell Motil* 2:549–572.
38. Fliegauf M, Benzing T, Omran H (2007) When cilia go bad: Cilia defects and ciliopathies. *Nat Rev Mol Cell Biol* 8:880–893.
39. Omran H, et al. (2008) *Ktu/PF13* is required for cytoplasmic pre-assembly of axonemal dyneins. *Nature* 456:611–616.
40. Sanderson MJ, Sleigh MA (1981) Ciliary activity of cultured rabbit tracheal epithelium: Beat pattern and metachrony. *J Cell Sci* 47:331–347.
41. Nonaka S, et al. (1998) Randomization of left-right asymmetry due to loss of nodal cilia generating leftward flow of extraembryonic fluid in mice lacking KIF3B motor protein. *Cell* 95:829–837.
42. Bartoloni L, et al. (2002) Mutations in the *DNAH11* (axonemal heavy chain dynein type 11) gene cause one form of situs inversus totalis and most likely primary ciliary dyskinesia. *Proc Natl Acad Sci USA* 99:10282–10286.
43. Schwabe GC, et al. (2008) Primary ciliary dyskinesia associated with normal axoneme ultrastructure is caused by *DNAH11* mutations. *Hum Mutat* 29:289–298.
44. Suryavanshi S, et al. (2010) Tubulin glutamylation regulates ciliary motility by altering inner dynein arm activity. *Curr Biol* 20:435–440.
45. Kubo T, Yanagisawa HA, Yagi T, Hirono M, Kamiya R (2010) Tubulin polyglutamylation regulates axonemal motility by modulating activities of inner-arm dyneins. *Curr Biol* 20: 441–445.
46. Ostrowski LE, et al. (2002) A proteomic analysis of human cilia: Identification of novel components. *Mol Cell Proteomics* 1:451–465.
47. Pazour GJ, Agrin N, Leszyk J, Witman GB (2005) Proteomic analysis of a eukaryotic cilium. *J Cell Biol* 170:103–113.
48. Sugino K, Naitoh Y (1982) Simulated cross-bridge patterns corresponding to ciliary beating in *Paramecium*. *Nature* 295:609–611.
49. Dirksen ER, Zeira M (1981) Microtubule sliding in cilia of the rabbit trachea and oviduct. *Cell Motil* 1:247–260.
50. Ikegami K, et al. (2008) TTLL10 is a protein polyglycylase that can modify nucleosome assembly protein 1. *FEBS Lett* 582:1129–1134.
51. Ikegami K, Setou M (2009) TTLL10 can perform tubulin glycylation when co-expressed with TTLL8. *FEBS Lett* 583:1957–1963.